

# Main-sequence variable stars in young open cluster NGC 1893

Sneh Lata<sup>1\*</sup>, Ram Kesh Yadav<sup>1</sup>, A. K. Pandey<sup>1</sup>, Andrea Richichi<sup>2</sup>, C. Eswaraiah<sup>1,3</sup>,  
Brajesh Kumar<sup>1,4</sup>, Norbert Kappelman<sup>5</sup> and Saurabh Sharma<sup>1</sup>

<sup>1</sup>*Aryabhata Research Institute of Observational Sciences, Manora Peak, Nainital 263002, Uttarakhand, India*

<sup>2</sup>*National Astronomical Research Institute of Thailand, 191 Siriphanich Bldg., Huay Kaew Rd., Suthep, Muang, Chiang Mai 50200, Thailand*

<sup>3</sup>*Institute of Astronomy, National Central University, 300 Zhongda Rd, Zhongli, Taoyuan Country 32054, Taiwan*

<sup>4</sup>*Institut d'Astrophysique et de Géophysique, Université de Liège, Allée du 6 Août 17, Bât B5c, 4000 Liège, Belgium*

<sup>5</sup>*Institute of Astronomy and Astrophysics, Sand 1, 72076, Tübingen, Germany*

Accepted ———. Received ———;

## ABSTRACT

In this paper we present time series photometry of 104 variable stars in the cluster region NGC 1893. The association of the present variable candidates to the cluster NGC 1893 has been determined by using  $(U - B)/(B - V)$  and  $(J - H)/(H - K)$  two colour diagrams, and  $V/(V - I)$  colour magnitude diagram. Forty five stars are found to be main-sequence variables and these could be B-type variable stars associated with the cluster. We classified these objects as  $\beta$  Cep, slowly pulsating B stars and new class variables as discussed by Mowlavi et al. (2013). These variable candidates show  $\sim 0.005$  to  $\sim 0.02$  mag brightness variations with periods of  $< 1.0$  d. Seventeen new class variables are located in the  $H - R$  diagram between the slowly pulsating B stars and  $\delta$  Scuti variables. Pulsation could be one of the causes for periodic brightness variations in these stars. The X-ray emission of present main-sequence variables associated with the cluster lies in the saturated region of X-ray luminosity versus period diagram and follows the general trend by Pizzolato et al. (2003).

**Key words:** Open cluster: NGC 1893 – colour–magnitude diagram: Variables-main sequence stars-B type

## 1 INTRODUCTION

The aim of the present study is to analyze the light curves of those stars which lie in the upper part of the main-sequence (MS) in the colour-magnitude diagram (CMD) of NGC 1893. The upper part of the MS consists of stars of spectral type O to A. The brightness variation in OB supergiants, early B-type stars, Be stars, mid to late B-type stars occurs mostly due to the pulsations (Stankov & Handler 2005; Kiriakidis et al. 1992; Moskalik & Dziembowski 1992). Pulsating variable stars expand and contract in a repeating cycle of size changes. The different types of pulsating variables are distinguished by their periods of pulsation and the shapes of their light curves. These could be  $\beta$  Cep, slowly pulsating B (SPB),  $\delta$  Scuti stars etc. The  $\beta$  Cep stars are pulsating MS variables and found to be lying above the upper MS in the  $H - R$  diagram with early B spectral types (Handler & Meingast 2011). These have periods and amplitude in the range of 0.1 - 0.6 d and 0.01 to 0.3 mag, respectively.

The SPB stars lie just below the instability strip of  $\beta$  Cep variables (Waelkens 1991). The SPB stars are nearly perfectly confined to the main-sequence band (e.g., De Cat et al. 2004). The SPB stars are less massive ( $3-7 M_{\odot}$ ) in comparison to  $\beta$  Cep stars ( $8-18 M_{\odot}$ ). The effective temperature of known SPB stars lies in the range of 10000 to 20000 K. The well known Kappa mechanism (Dziembowski et al. 1993; Gautschi & Saio 1993) is the reason for the periodic brightness variation in these stars. The SPB stars are slow pulsator with period of more than 0.5 d. Theoretical instability strip of SPB stars overlap with instability strip of  $\beta$  Cep stars. Waelkens et al. (1998) classified a huge number of B-type stars as new SPB stars using the Hipparcos mission.

Another class of stars populating with the B-type MS are the Be stars. They are defined as non- supergiant B star with one or more Balmer lines in their emission. Classical Be stars are physically known as rapidly rotating B-type stars with line emission. As pulsating Be stars occupy the same region of the  $H - R$  diagram as  $\beta$  Cep and SPB stars, it is generally assumed that pulsations in Be stars have the

\* E-mail: sneh@aries.res.in

same origin as the case of  $\beta$  Cep and SPB stars (Diago et al. 2008).

The another group of pulsation variables is  $\gamma$  Dordus (period: 0.3-1.0 d). They are found to be located below the instability strip of  $\delta$  Scuti stars. The instability strip of  $\gamma$  Dordus overlaps with instability strip of  $\delta$  Scuti. The  $\delta$  Scuti stars (these are short period variables with periods lying in the range of 0.03 to 0.3 d) are part of the classical instability strip where Cepheids are found and these Cepheids are radially pulsating, high luminosity (classes Ib-II) variables with periods in the range of 1-135 days and amplitudes from several hundredths to  $\sim 2$  mag in  $V$  (the amplitudes are greater in the  $B$  band). The spectral type of these objects at maximum light is F whereas at the minimum, the spectral types are G-K. The longer the period of light variation, the later is the spectral type.

In addition to above discussions we would like to give a brief description of previous studies on B-type stars' variability. The study of pulsating B-stars having same age and chemical composition in young open clusters provides understanding to interpret variability (Handler et al. 2008; Majewska et al. 2008; Michalska et al. 2009; Handler & Meingast 2011; Jerzykiewicz et al. 2011; Saesen et al. 2013; Balona et al. 1997; Gruber et al. 2012). Saesen et al. (2013) using the photometric study of the B-type stars in NGC 884 combined with their recent spectroscopic observations offer an interesting and different approach to the advancement of understanding of these young massive objects. Saesen et al. (2010) presented differential time-resolved multi-colour CCD photometry of NGC 884 cluster that leads to the identification of 36 multi-periodic and 39 mono-periodic B-stars, 19 multi-periodic and 24 mono-periodic A- and F-stars, and 20 multi-periodic and 20 mono-periodic variable stars of unknown nature. Saio et al. (2006) used MOST (Microvariability and Oscillations of Stars) satellite to detect variability in supergiant star HD 163899 (B2 Ib/II), and they found 48 frequencies with amplitudes of a few millimagnitudes (mmag) and less. The frequency range is similar to g- and p-mode pulsations.

Balona et al. (2011) presented Kepler observations of variability in B-type stars. They presented the light curves of 48 B-type stars. They find no evidence for pulsating stars between the cool edge of the SPB and the hot edge of the  $\delta$  Scuti instability strips. Recently, McNamara et al. (2012) analyzed the light curves of 252 B-star candidates in the Kepler data base to further characterize B star's variability and to increase the sample of variable B stars for future study. They classified stars as either constant light emitters,  $\beta$  Cep stars, SPB stars, hybrid pulsators, binaries or stars whose light curves are dominated by rotation, hot subdwarfs, or white dwarfs. Mowlavi et al. (2013) in the case of open cluster NGC 3766 found large population of new variable stars between the red end of SPB type stars and the blue end of the  $\delta$  Scuti type stars where no pulsations are expected to occur on the basis of standard models. They argued that pulsation could be one of the reasons for showing brightness variation in these stars.

Yang et al. (2013) also presented CCD time series photometric observations for the stars in the open clusters NGC 7209, NGC 1582 and Dolidize 18 and found only one star which could be B-type pulsating star. Jerzykiewicz et al. (2003) presented results of a search for variable stars in the

field of the young open cluster NGC 2169 and found two  $\beta$  Cep stars and other type stars. Diago et al. (2008) have also detected absorption-line B and Be stars in the SMC showing short period variability. Briquet et al. (2001) studied B-type star HD 131120 and found that this star is monophasic with a period of 1.569 d. They interpreted the variability of this star in terms of a non-radial g-mode pulsation model as well as in terms of a rotational modulation model. They found that rotational modulation model was able to explain the observed line profile variations of the star. Luo et al. (2012) carried out  $BV$  CCD photometric observations of the open cluster NGC 7654, a young open cluster located in the Cassiopeia constellation, to search for variable stars and detected 18 SPB stars. They find that the multi-mode pulsation is more common in the upper part of the MS and g-mode MS pulsating variables probably follow a common period-luminosity relation.

In the light of above discussions we aimed to search for variable stars in the upper part of MS of NGC 1893. The NGC 1893 cluster is a young open cluster which is associated with nebulae and obscured by dust clouds. Detailed study of the NGC 1893 on the basis of photometric data has been carried out by Sharma et al. (2007) and Pandey et al. (2013). Marco & Negueruela (2002a) have found the presence of Herbig Ae/Be in the vicinity of O-type stars and B-type MS stars of later spectral type. On the basis of spectroscopic survey in the region of NGC 1893 Marco & Negueruela (2002b) suggest that both Herbig Be stars and classical Be stars are present in NGC 1893. Zhang et al. (2008) and Lata et al. (2012) identified a few B-type variable stars in the cluster NGC 1893. The previous studies show that NGC 1893 is one of the richest clusters to study the variable stars. This paper is in continuation of our efforts to study the MS variable stars in young clusters. In our earlier papers (Lata et al. 2011, 2012), we have presented time series photometry of PMS variable candidates.

The observations of NGC 1893 in the  $V$  band have been carried out on 16 nights during December 2007 to January 2013 in order to identify and characterize the variable stars in the NGC 1893 region. In Section 2 we describe the observations and data reduction procedure. In Section 3 we discuss the cluster membership of detected variables using  $(U - B)/(B - V)$ ,  $(J - H)/(H - K)$  two colour diagram (TCD) and  $V/(V - I)$  CMD. Section 4 deals with period determination of variables. Section 5 describes luminosity and temperature of the stars. The variability characteristics of the stars are discussed in Section 6. We discuss X-ray luminosity and period for the variables in Section 7. Finally, we summarise our results in Section 8.

## 2 OBSERVATIONS AND DATA REDUCTION

The present work uses observations made from two telescopes; 104-cm ARIES telescope and 130-cm Devasthal telescope. The details of these two telescopes and instrument are given below. The photometric observations of the NGC 1893 region were carried out in the  $V$ -band on 15 nights and in the  $I$ -band on two nights during 2007 December 05 to 2013 January 05 using a  $2048 \times 2048$  CCD camera attached to the 104-cm Sampurnanand ARIES telescope at Nainital. The field of view is  $\sim 13' \times 13'$  and the scale is  $\sim 0.76''/\text{pixel}$  in

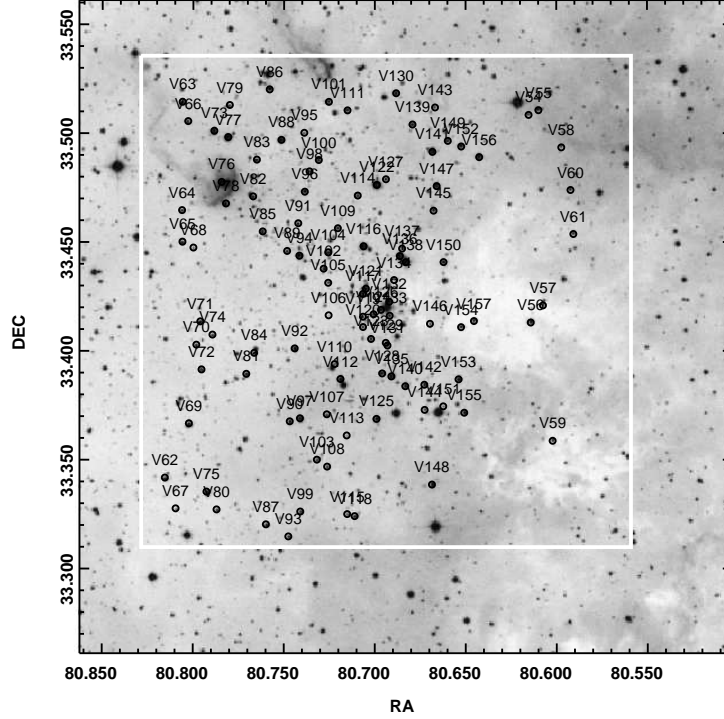


**Figure 1.** The image of NGC 1893 of  $18 \times 18$  arcmin<sup>2</sup> taken from the DSS-R. The observed region from 104 cm is shown by rectangle. The variable candidates detected in the present work are encircled and labeled with numbers.

**Table 1.** Log of the observations. N and Exp. represent number of frames obtained and exposure time respectively.

S. No.	Date of observations	Object	V (N×Exp.)	I (N×Exp.)
1	05 Dec 2007	NGC 1893	3×40s	-
2	08 Dec 2007	NGC 1893	3×50s	-
3	07 Jan 2008	NGC 1893	2×40s	-
4	10 Jan 2008	NGC 1893	3×50s	-
5	12 Jan 2008	NGC 1893	80×50s	-
6	14 Jan 2008	NGC 1893	70×40s	-
7	29 Oct 2008	NGC 1893	97×50s	-
8	21 Nov 2008	NGC 1893	137×50s	2×50s
9	27 Jan 2009	NGC 1893	5×50s	-
10	28 Jan 2009	NGC 1893	5×50s	-
11	19 Feb 2009	NGC 1893	5×50s	-
12	20 Feb 2009	NGC 1893	3×50s	5×50s
13	20 Feb 2009	SA 98	5×90s	5×60s
14	31 Oct 2010	NGC 1893	3×50s	-
15	22 Dec 2012	NGC 1893	323×50s	-
16	05 Jan 2013	NGC 1893	80×50s	-

$2 \times 2$  pixel binning mode. The central position on the sky was close to RA (2000) =  $05^h 22^m 42^s$  and Dec (2000) =  $+33^\circ 25' 00''$  for all the frames.

In addition, we have also observed the region in V-band on 22 December 2012 using 130-cm Devasthal telescope. The 130-cm Devasthal telescope uses  $2048 \times 2048$  CCD camera having pixel size of  $13.5 \mu\text{m}$  mounted at the f/4 Cassegrain

focus of the telescope. With 0.54 arcsec per pixel plate scale, the entire chip covers a  $\sim 18 \times 18$  arcmin<sup>2</sup> field of view on the sky. Fig. 1, image taken from Digital Sky Survey (DSS), displays the observed region of NGC 1893. The observations of NGC 1893 consist of a total of 824 CCD images in the V-band. Bias and twilight flats were also taken along with the target field. The log of the observations is given in Table 1.

## 2.1 Photometry and variable identification

The preprocessing of the CCD images was performed using the IRAF<sup>1</sup> and the instrumental magnitude of the stars were obtained using the DAOPHOT package (Stetson 1987). The details of the procedure can be found in our earlier work (Lata et al. 2012). We have considered only those stars for further study which have at least 100 observations. The variable candidates were identified by inspecting their light curves (Sariya, Lata & Yadav 2014). The observations taken during December 2007 to October 2010 have already been used in our previous study (Lata et al. 2012) to identify the PMS variable stars. Present study focuses mainly on the MS stars. We have identified 104 new variable candidates. The identification number, coordinates and present

<sup>1</sup> IRAF is distributed by the National Optical Astronomy Observatory, which is operated by the Association of Universities for Research in Astronomy (AURA) under cooperative agreement with the National Science Foundation.

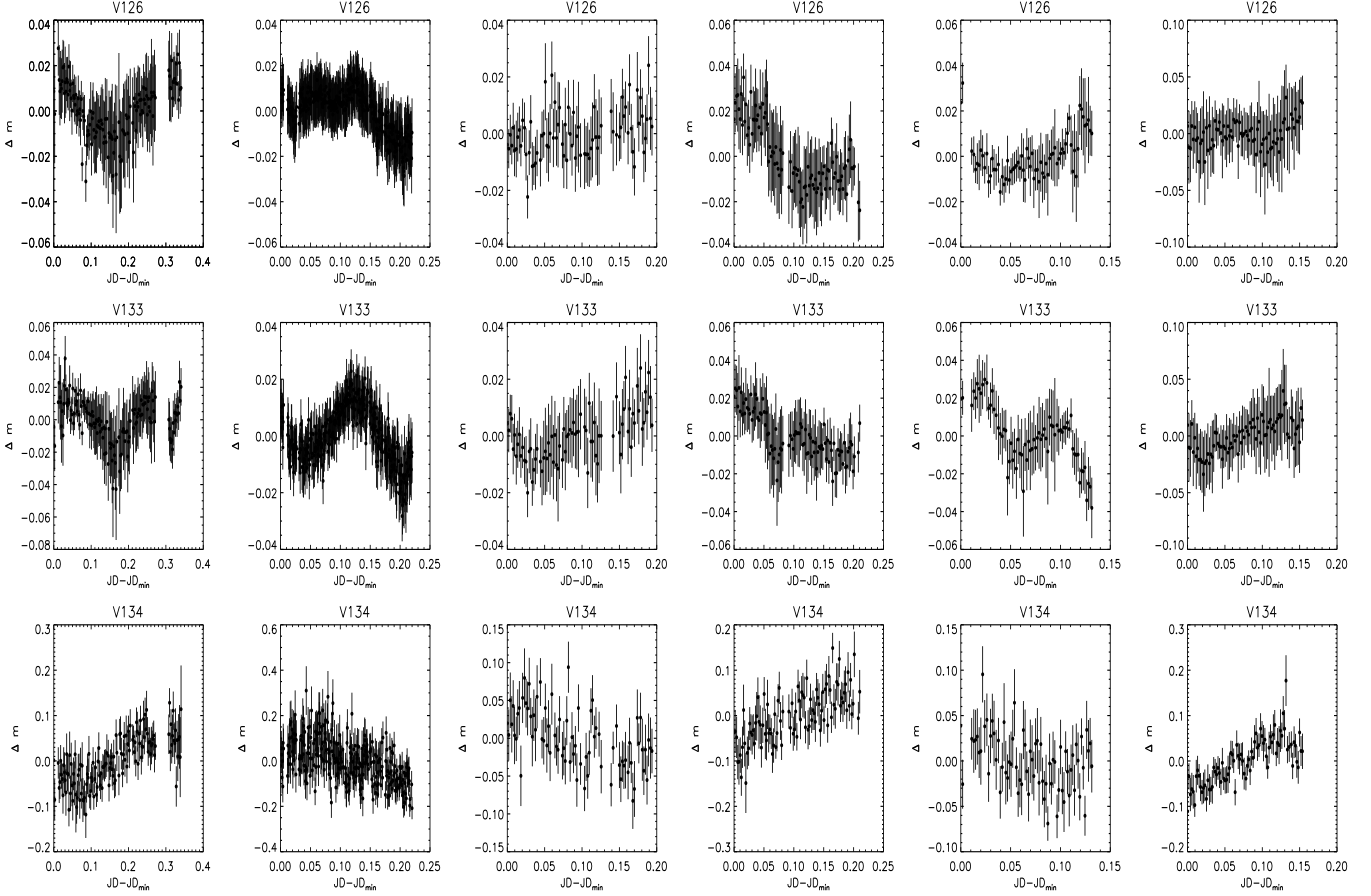


**Figure 2.** Sample light curves of a few variable stars identified in the present work. The  $\Delta m$  represents the differential magnitude in the sense that variable minus comparison star. The complete figure is available online.

*VI* photometric data for these variable stars are given in Table 2. The identification number is in continuation of previous work (Lata et al. 2012). Sample light curves of a few variables are shown in Fig. 2. The complete Fig. 2. is available in electronic form. Table 2 also lists *NIR* data taken from Prisinzano et al. (2011) and 2MASS catalogue (Cutri et al. 2003). The procedure of standardization has been given in Lata et al. (2012). The variable candidates identified in the present sample are marked in Fig. 1.

### 3 MEMBERSHIP

The  $(U - B)/(B - V)$  and  $(J - H)/(H - K)$  TCD, and  $V/(V - I)$  CMD have been used to find out the association of the identified variables with the cluster NGC 1893 and to know the nature of the present variable candidates.

#### 3.1 $(U - B)/(B - V)$ and $(J - H)/(H - K)$ two colour Diagrams

The  $U - B/B - V$  TCD for variable candidates is shown in Fig. 3. The *UBV* data for 92 common variable candidates have been taken from Sharma et al. (2007). Since present sample consists of 104 stars, for remaining 12 stars *UBV*

data have been taken from Massey et al. (1995). The distribution of stars in the  $(U - B)/(B - V)$  TCD indicates a variable reddening in the cluster region with  $E(B - V)$  from  $\sim 0.4$  to  $0.7$  mag. The majority of the stars having  $E(B - V)$  from  $\sim 0.4$  to  $0.7$  mag have  $(B - V)$  colours  $\lesssim 0.6$  mag. These could be OB-population of the NGC 1893 cluster. To further classify these stars we used  $(J - H)/(H - K)$  TCD as shown in Fig. 4. The *JHK* data have been taken from Prisinzano et al. (2011) and 2MASS. Out of 104 variables 98 stars have their *JHK* counter parts. The *JHK* data catalogued by Prisinzano et al. (2011) are in MKO system which were converted to 2MASS system using relations given on the website<sup>2</sup>. After that *JHK* data from both the catalogues (Prisinzano catalogue and 2MASS catalogue) were transformed to CIT system using the relations given on the above mentioned website. The solid and long dashed lines in Fig. 4 represents unreddened MS and giant loci (Bessell & Brett 1988) respectively. The dotted line indicates the intrinsic locus of classical T-tauri stars (CTTSs) (Meyer et al. 1997). The parallel dashed lines are the reddening vectors drawn from the tip (spectral type M4) of the giant branch (‘left reddening line’), from the base (spectral type A0) of the main-sequence branch (‘middle reddening line’) and from the tip of the intrinsic CTTS line (‘right reddening line’). The extinction ra-

<sup>2</sup> <http://www.astro.caltech.edu/jmc/2mass/v3/transformations/>

**Table 2.** The present photometric data, NIR data, period, amplitude and classification of 104 variables in the region of NGC 1893. The NIR data have been taken from Prisinzano et al. (2011) and 2MASS point source catalogue (Cutri et al. 2003).

ID	$\alpha$ 2000 degree	$\delta$ 2000 degree	V mag	V - I mag	J mag	H mag	K mag	[Jmko] mag	[Hmko] mag	[Kmkko] mag	[period] day	[Amp.] mag	Classification.
V54	80.61530	33.50847	15.489	0.975	14.006	13.622	13.524	-	-	-	0.211	0.015	Field
V55	80.60988	33.51063	14.438	1.260	12.417	11.848	11.688	13.958	13.394	13.069	0.159	0.016	Field
V56	80.61419	33.41311	12.777	0.593	11.754	11.626	11.526	-	-	-	0.345	0.010	Field
V57	80.60744	33.42097	14.617	0.813	13.279	13.050	12.948	-	-	-	0.236	0.009	Field
V58	80.59730	33.49355	15.889	0.970	14.278	13.916	13.742	-	-	-	0.141	0.022	Field
V59	80.60219	33.35877	15.175	0.978	13.576	13.218	13.128	-	-	-	0.244	0.011	Field
V60	80.59224	33.47397	14.531	0.559	13.617	13.485	13.345	-	-	-	0.236/0.538	0.012	MS
V61	80.59069	33.45375	15.183	0.922	13.708	13.370	13.280	13.698	13.395	13.261	0.211	0.012	Field
V62	80.81544	33.34186	13.674	1.004	12.030	11.656	11.581	-	-	-	0.280	0.010	Field
V63	80.80588	33.51449	14.498	1.628	11.825	11.175	11.005	-	-	-	0.376	0.010	PMS
V64	80.80611	33.46472	15.225	1.790	12.138	11.386	11.187	12.140	12.027	13.766	0.311	0.015	PMS
V65	80.80588	33.45022	14.445	0.907	13.008	12.716	12.617	-	-	-	0.343	0.013	Field
V66	80.80278	33.50561	15.025	1.137	13.248	12.836	12.714	-	-	-	0.233	0.011	Field
V67	80.80950	33.32772	16.281	1.179	-	-	-	-	-	-	0.079	0.020	Field
V68	80.79985	33.44752	16.984	1.173	15.068	14.587	14.510	-	-	-	0.072	0.031	Field
V69	80.80225	33.36680	12.398	0.436	11.731	11.647	11.596	-	-	-	0.486	0.008	MS
V70	80.79819	33.40291	14.506	0.757	13.183	12.902	12.786	13.193	13.216	12.745	0.535/0.434	0.016	MS
V71	80.79602	33.41363	14.438	0.522	13.627	13.423	13.401	-	-	-	0.520/0.638	0.014	MS
V72	80.79533	33.39155	14.212	0.503	13.258	13.105	13.060	13.518	13.281	13.054	0.209	0.011	MS
V73	80.78839	33.50119	12.520	0.951	10.785	10.405	10.013	10.905	10.434	10.116	0.269	0.007	Herbig Ae/Be
V74	80.78932	33.40755	14.224	0.715	12.985	12.699	12.574	13.109	12.887	12.666	0.249	0.008	MS
V75	80.79255	33.33544	13.663	1.495	10.595	9.953	9.791	-	-	-	0.238	0.009	PMS
V76	80.78433	33.47766	14.743	1.326	11.789	10.949	10.255	14.622	13.723	13.018	0.255	0.034	PMS
V77	80.78074	33.49830	11.876	1.644	9.196	8.457	8.295	-	-	-	0.229	0.007	PMS
V78	80.78194	33.46780	13.261	0.506	-	-	-	12.756	12.502	12.468	0.423/0.655/0.575	0.019	MS
V79	80.77986	33.51302	14.712	0.614	-	-	-	14.220	13.756	13.783	0.290	0.017	MS
V80	80.78700	33.32725	15.637	1.691	12.689	11.995	11.784	14.172	14.237	-	0.233	0.015	PMS
V81	80.77069	33.38955	14.165	0.471	-	-	-	-	-	-	0.177	0.007	MS
V82	80.76699	33.47105	13.670	0.571	12.771	12.574	12.470	16.247	15.334	14.684	0.510	0.006	MS
V83	80.76494	33.48794	13.890	0.567	13.052	12.991	12.857	-	-	-	0.458/0.478	0.007	MS
V84	80.76638	33.39919	14.655	0.507	-	-	-	-	-	-	0.310/0.354	0.010	MS
V85	80.76171	33.45497	14.203	0.909	-	-	-	-	-	-	0.287	0.006	Field
V86	80.75791	33.52019	13.037	1.826	10.296	9.641	9.471	-	-	-	0.246	0.010	PMS
V87	80.75986	33.32041	14.625	2.400	10.359	9.365	9.056	-	-	-	0.260	0.011	PMS
V88	80.75141	33.49702	12.337	0.556	11.636	11.529	11.428	-	-	-	0.466/0.389	0.013	MS
V89*	80.74827	33.44599	14.238	0.549	13.282	13.199	13.047	-	-	-	0.586	0.016	MS
V90	80.74678	33.36774	14.653	0.742	13.700	13.529	13.432	-	-	-	0.279/0.254	0.009	MS
V91*	80.74214	33.45872	14.559	0.540	12.395	12.255	12.209	-	-	-	0.511/0.576	0.016	MS
V92*	80.74407	33.40124	13.130	0.438	12.395	12.255	12.209	13.468	13.178	13.038	0.594/0.474	0.016	MS
V93	80.74752	33.31486	14.838	0.829	13.421	13.192	13.053	-	-	-	0.327	0.012	Field
V94*	80.74150	33.44383	12.122	0.421	11.460	11.32	11.261	11.781	12.814	11.746	0.603/0.376/0.670/0.875	0.007	MS
V95	80.73883	33.50027	15.623	0.875	14.175	13.966	13.833	-	-	-	0.194	0.012	Field
V96	80.73855	33.47322	13.520	1.114	11.758	11.263	11.160	11.640	11.333	11.101	0.250	0.006	Field
V97	80.74116	33.36914	12.535	0.384	11.911	11.816	11.812	-	-	-	0.483/3.75	0.007	MS
V98	80.73594	33.48255	14.719	0.659	13.668	13.558	13.436	-	-	-	0.458/0.478/0.622	0.019	MS
V99	80.74097	33.32630	15.225	0.884	13.738	13.444	13.313	-	-	-	0.179	0.013	Field
V100	80.73085	33.48777	14.451	1.212	12.478	12.094	11.943	-	-	-	0.137	0.007	Field
V101	80.72528	33.51449	15.017	1.737	12.181	11.472	11.053	12.097	11.482	11.143	0.245	0.010	PMS
V102	80.72816	33.43786	14.380	0.686	13.235	13.040	12.918	-	-	-	0.424/0.633	0.011	MS
V103	80.73185	33.35013	15.560	1.244	13.418	12.844	12.708	-	-	-	0.303	0.014	Field
V104*	80.72563	33.44538	13.417	0.440	12.798	12.677	12.619	-	12.615	12.509	0.476/0.653	0.006	MS
V105	80.72566	33.43138	15.765	0.897	14.261	13.871	13.822	-	-	-	0.294	0.013	Field
V106	80.72541	33.41644	18.507	1.784	15.149	14.463	14.197	15.136	14.475	14.099	0.187	0.079	PMS
V107	80.72641	33.37097	14.861	0.837	13.434	13.113	13.068	-	-	-	0.268	0.009	Field
V108	80.72621	33.34694	15.449	1.105	13.524	13.191	13.031	15.781	15.704	15.244	0.179	0.014	Field
V109*	80.72033	33.45644	14.609	0.582	13.681	13.376	13.232	13.685	13.424	13.277	0.511/0.623	0.014	MS
V110	80.72211	33.39405	16.764	1.130	-	-	-	15.961	14.737	15.011	0.068	0.039	Field
V111	80.71502	33.51058	13.979	0.971	12.425	12.164	12.042	-	-	-	0.224	0.007	Field
V112*	80.71888	33.38719	12.405	0.353	11.822	11.76	11.713	-	-	-	0.325	0.009	MS
V113	80.71544	33.36125	18.006	1.833	14.776	13.956	13.702	14.645	13.907	13.724	0.279	0.068	PMS
V114	80.70938	33.47144	14.420	0.866	13.075	12.797	12.711	-	-	-	0.380	0.007	Field
V115	80.71516	33.32513	16.180	1.285	13.950	13.507	13.375	-	-	-	0.354	0.020	Field
V116*	80.70619	33.44816	11.168	0.353	10.716	10.69	10.673	-	-	-	0.505/0.616/0.455	0.015	MS
V117	80.70655	33.42625	12.722	0.554	11.806	11.665	11.566	12.128	12.254	11.851	0.596	0.018	MS
V118	80.71108	33.32419	14.148	0.970	12.479	12.145	12.020	-	-	-	0.182	0.012	Field
V119	80.70652	33.41580	15.039	1.069	13.238	12.760	12.653	-	-	-	0.269	0.011	Field
V120	80.70647	33.41105	15.093	0.881	13.627	13.263	13.129	14.277	13.884	13.722	0.209	0.012	Field
V121	80.70488	33.42866	13.702	0.518	-	-	-	13.197	13.008	12.555	0.448	0.009	MS
V122	80.69889	33.47633	11.043	1.373	8.816	8.218	8.059	-	-	-	0.195	0.008	Field
V123	80.70205	33.40558	14.454	0.555	13.428	13.337	13.221	13.782	14.053	13.376	0.190	0.008	MS
V124**	80.70066	33.41694	15.351	1.525	12.771	12.147	11.971	13.865	12.701	12.327	0.242	0.015	PMS
V125	80.69908	33.36886	12.574	0.950	10.921	10.582	10.494	-	-	-	0.436	0.008	MS
V126	80.69660	33.41894	13.061	0.466	-	-	-	12.439	12.501	12.326	0.501/0.416/0.732	0.010	MS
V127	80.69386	33.47894	14.373	0.949	12.902	12.584	12.502	-	-	-	0.177	0.007	Field
V128*	80.69594	33.38975	13.851	0.683	12.578	12.263	12.122	12.632	12.275	12.160	0.269	0.007	MS
V129**	80.69394	33.40380	14.385	0.784	12.938	12.719	12.604	13.150	13.145	12.655	0.309	0.009	MS
V130	80.68824	33.51844	13.671	0.906	12.269	11.964	11.896	12.173	11.885	11.802	0.211	0.010	Field
V131**	80.69300	33.40258	14.748	1.205	12.604	12.104	11.799	12.761	12.442	11.857	0.208	0.010	PMS
V132	80.69205	33.42266	12.482	0.550	-	-	-	11.485	11.361	11.266	0.554/0.570	0.008	MS
V133*	80.69178	33.41624	13.925	0.666	-	-	-	14.571	13.923	13.605	0.485/0.467	0.012	MS
V134	80.68939	33.43264	17.825	1.585	11.885	11.778	11.778	14.819	14.194	13.989	0.376	0.067	Field
V135*	80.69088	33.38838	12.638	0.442	10.703	10.65	10.621	-	-	-	0.353	0.007	MS
V136*	80.68619	33.44366	11.315	0.445	-	-	-	10.545	10.508	10.628	0.541/0.429/0.646	0.008	MS
V137	80.68497	33.44708	16.236	1.251	-	-	-	-	-	-	0.382	0.021	Field
V138*	80.68297	33.44086	10.218	0.434	9.648	9.633	9.584	-	9.394	9.532	0.570/0.593/0.456	0.006	MS
V139	80.67925	33.50408	13.778	0.827	12.481	12.226	12.143	-	-	-	0.411/0.333	0.015	MS

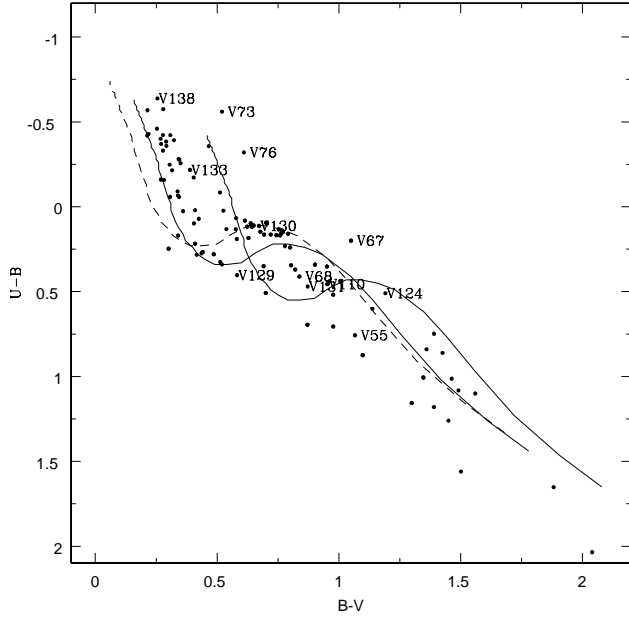


**Figure 3.**  $U - B/B - V$  two colour diagram variable stars. The  $UBV$  data have been taken from Sharma et al. (2007) and Massey et al. (1995). The solid curve represents the ZAMS by Girardi et al. (2002) shifted along the reddening vector of 0.72 for  $E(B - V)_{min} = 0.4$  mag and  $E(B - V)_{max} = 0.7$  mag. The dashed curve represents ZAMS by Girardi et al. (2002) for the foreground field population having  $E(B - V) = 0.30$  mag. The stars labeled are discussed in section 6.

tios  $A_J/A_V = 0.265$ ,  $A_H/A_V = 0.155$  and  $A_K/A_V = 0.090$  have been adopted from Cohen et al. (1981). The sources lying in ‘F’ region could be either field stars (MS stars, giants) or Class III and Class II sources with small NIR excesses. The sources lying in the ‘T’ region are considered to be mostly CTTSs (Class II objects). The  $(J - H)/(H - K)$  TCD shows that the majority of the variable candidates are located below TTS locus and these should be MS stars.

### 3.2 $V/V - I$ colour-magnitude diagram

The  $V/V - I$  CMD for all the variable candidates have been plotted in Fig 5. In Fig. 5 we have also plotted theoretical isochrone for 4 Myr for  $Z=0.02$  (continuous line) by Girardi et al. (2002) and PMS isochrones for various ages as well as evolutionary tracks for various masses by Siess et al. (2000). All the isochrones and evolutionary tracks are corrected for the distance (3.25 kpc) and minimum reddening  $E(V - I)=0.50$  mag. The minimum value of  $E(V - I)$  has been estimated using the relation  $E(V - I)/E(B - V) = 1.25$  and  $E(B - V) = 0.40$  mag.

The identified variables are classified as MS, PMS and field stars on the basis of their location in the  $(U - B)/(B - V)$ ,  $(J - H)/(H - K)$  TCDs and  $V/(V - I)$  CMD and the classification is given in the 14th column of Table 2.

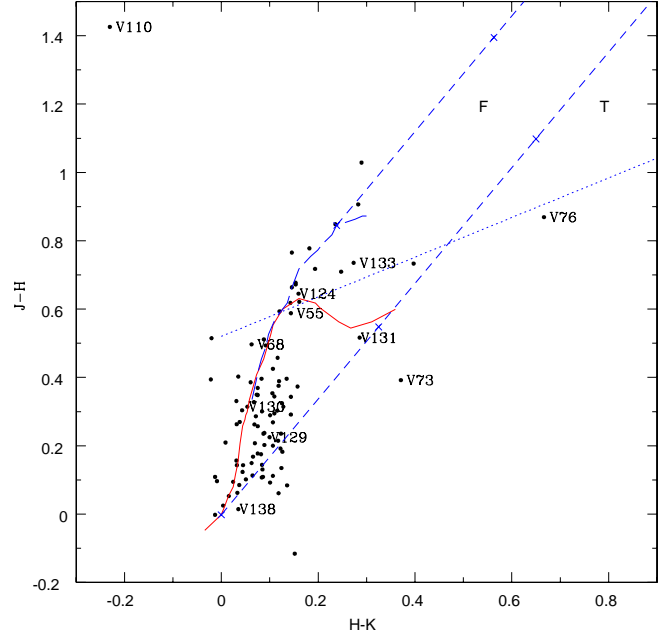


**Figure 4.**  $(J - H)/(H - K)$  TCD for variable stars lying in the field of  $13 \times 13$  arcmin of NGC 1893.  $JHK$  data have been taken from Prisinzano et al. (2011). The sequences for dwarfs (solid curve) and giants (long dashed curve) are from Bessell & Brett (1988). The dotted curve represents the locus of TTSs (Meyer et al. 1997). The small dashed lines represent the reddening vectors (Cohen et al. 1981). The crosses on the reddening vectors represent an increment of visual extinction of  $A_V = 5$  mag. The stars labeled are discussed in section 6.

## 4 PERIOD DETERMINATION

We used the Lomb-Scargle (LS) periodogram (Lomb 1976; Scargle 1982) to determine the most probable period of a variable star. The LS method is useful to estimate periodicities even in the case of unevenly spaced data. We used the algorithm available at the Starlink<sup>3</sup> software database. The periods were further verified with the software period04<sup>4</sup> (Lenz & Breger 2005). The software period04 provides the frequency and semi-amplitude of the variability in a light curve. Periods derived from the LS method and Period04 generally matched well. The most probable periods with amplitude are listed in Table 2. The light curves of variable stars are folded with their estimated period. Sample phased light curves of identified MS, PMS and field stars are shown in Figs. 6, 7 and 8 respectively, where averaged differential magnitude in 0.01 phase bin along with  $\sigma$  error bars have been plotted. The phased light curves of all the MS, PMS and field variable stars are available online.

<sup>3</sup> <http://www.starlink.uk>

<sup>4</sup> <http://www.univie.ac.at/tops/Period04>

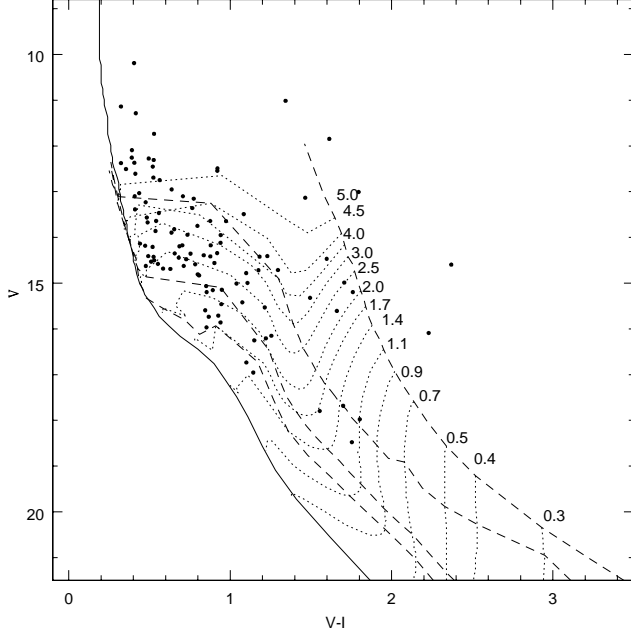


**Figure 5.**  $V/V-I$  colour-magnitude diagram of the cluster NGC 1893 for variable candidates. The ZAMS by Girardi et al. (2002) and PMS isochrones for 0.1, 1, 5, 10 Myrs by Siess et al. (2000) are shown. The dotted curves show PMS evolutionary tracks of stars of different masses. The isochrones and evolutionary tracks are corrected for the cluster distance and  $E(V-I) = 0.50$  mag.

## 5 $M_V/(B-V)_0$ AND LUMINOSITY ( $L/L_\odot$ ) VS. EFFECTIVE TEMPERATURE ( $T_{EFF}$ ) DIAGRAM

The  $M_V/(B-V)_0$  CMD for the identified MS and PMS stars is shown in Fig. 9. The intrinsic  $(B-V)$  colours of MS stars have been determined using Q-method as described by Gutierrez-Moreno (1975). For PMS stars we have used average reddening ( $E(B-V)=0.55$  mag) of the region. Fig. 10 shows  $\log(L/L_\odot)/\log T_{eff}$  diagram for the MS variables. The absolute magnitude  $M_V$  was converted to luminosity using the relations  $\log(L/L_\odot) = -0.4(M_{bol} - M_{bol,\odot})$ , and  $M_{bol} = M_V + BC$ , where BC is the bolometric correction. The bolometric magnitude  $M_{bol,\odot}$  for the Sun has been taken 4.73 mag (Torres 2010). To determine BC and effective temperature  $T_{eff}$  we used the relations between  $T_{eff}$ -intrinsic  $(B-V)$  colours, and between  $T_{eff}$ -BC by Torres (2010). The luminosity ( $\log L/L_\odot$ ),  $M_{bol}$  and  $\log T_{eff}$  and BC of MS stars are listed in Table 3.

## 6 VARIABILITY CHARACTERISTICS

### 6.1 MS variables

In this section we will characterize the MS variables identified in the present study. To characterize the variable stars we need period, amplitude and shape of the light curves. Additionally, the position of the variable stars in the  $H-R$  diagram is also needed to ascertain their nature. Fig. 10 shows the  $H-R$  diagram for variables along with the theoretical SPB instability (continuous curve), location of  $\beta$  Cep

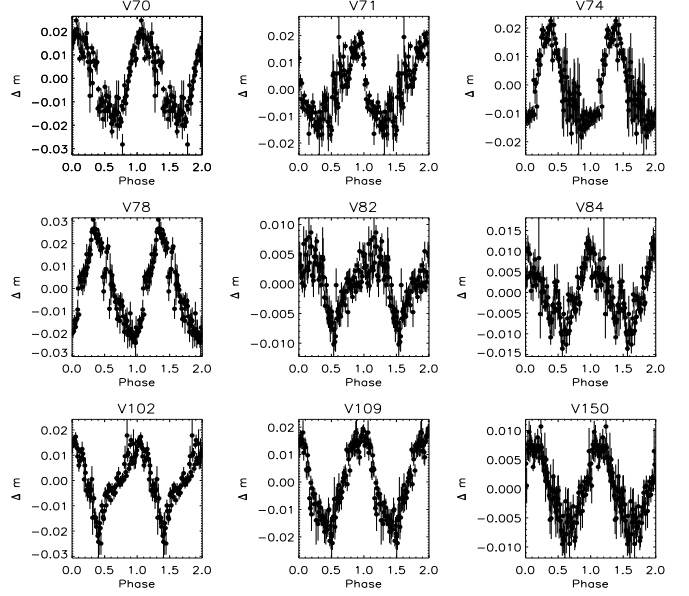


**Figure 6.** The sample phased light curves of MS variable stars. The complete figure is available electronic form only.

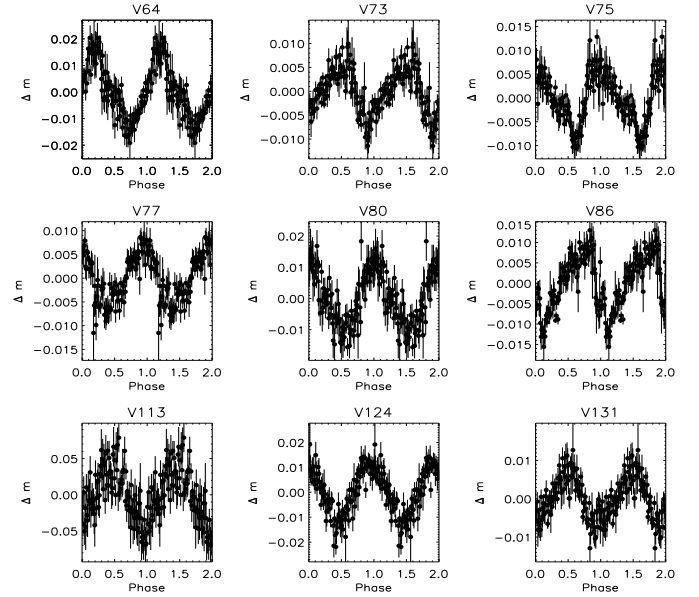


**Figure 7.** Same as Fig. 6 but for PMS variable stars. The complete figure is available electronic form only.

stars (dashed curve) and empirical  $\delta$  instability strip (dotted curve) taken from Balona et al. (2011; references therein).

Forty five stars are found to be of MS type stars. We find that the observed range of periods for these stars is between 0.17 to 0.6 d. The amplitude of these stars is of level of a few mmag). These could be  $\beta$  Cep, SPB and classical Be type stars. In the  $H-R$  diagram the lower limit of  $\log L/L_\odot$  for  $\beta$  Cep type is predicted as  $\gtrsim 3$ , whereas for SPB variables the lower limit of  $\log L/L_\odot$  as  $\sim 1.8$ . The  $\delta$  Scuti type stars have upper limit as  $\log L/L_\odot=1$ . There is about 2 mag gap between red end of SPB type stars and blue end of  $\delta$  Scuti type stars (Mowlavi et al. 2013). Mowlavi et

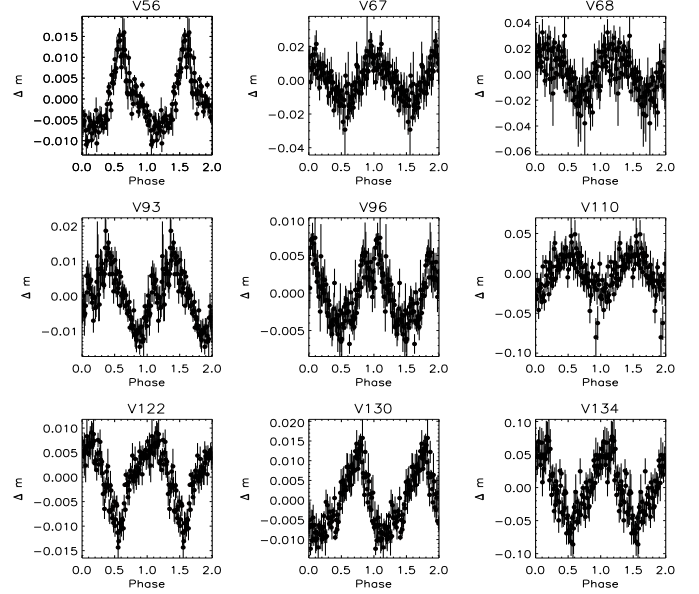


**Table 3.** The effective temperature  $T_{eff}$ , bolometric correction (BC), bolometric magnitude ( $M_{bol}$ ), luminosity ( $L$ ) and classification for MS stars.

ID	$\log T_{eff}$	BC	$M_{bol}$	$\log(L/L_{\odot})$	Classification
V60	3.988	-0.03125	0.7067	1.610	new
V69	4.203	-1.35900	-2.6790	2.965	SPB
V70	3.987	-0.07031	0.6997	1.613	new
V71	4.092	-0.60940	0.0886	1.857	new
V72	3.997	-0.09375	0.3563	1.750	new
V74	4.030	-0.28120	0.1937	1.815	new
V78	4.182	-1.16400	-1.6810	2.565	SPB
V79	4.058	-0.42190	0.5581	1.670	new
V81	4.089	-0.55470	-0.1487	1.952	new
V82	4.071	-0.50000	-0.5850	2.127	SPB
V83	4.131	-0.92190	-0.7899	2.209	SPB
V84	4.059	-0.54690	0.3631	1.748	new
V88	4.260	-1.50000	-2.9320	3.066	SPB
V89	4.043	-0.38280	0.0952	1.855	new
V90	4.050	-0.46090	0.4041	1.731	new
V91	4.080	-0.55470	0.2533	1.791	new
V92	4.206	-1.32800	-1.9910	2.689	SPB
V94	4.259	-1.63300	-3.2830	3.206	SPB
V97	4.208	-1.32800	-2.5790	2.924	SPB
V98	4.043	-0.31250	0.6455	1.635	new
V102	3.989	-0.02344	0.6006	1.653	new
V104	4.223	-1.32000	-1.6550	2.555	SPB
V109	4.069	-0.50000	0.3570	1.750	new
V112	4.218	-1.42200	-2.7830	3.006	SPB
V116	4.328	-2.07800	-4.6720	3.762	$\beta$ Cep
V117	4.179	-1.03100	-2.0690	2.720	SPB
V121	4.144	-0.96880	-1.0250	2.303	SPB
V123	3.983	-0.06250	0.6215	1.644	new
V125	4.078	-0.57810	-1.7990	2.612	SPB
V126	4.245	-1.36700	-2.0970	2.732	SPB
V128	4.142	-0.84380	-0.7797	2.205	SPB
V129	3.983	0.06250	0.6515	1.632	new
V132	4.168	-0.94530	-2.2320	2.786	SPB
V133	4.161	-1.01600	-0.8546	2.235	SPB
V135	4.223	-1.59400	-2.7500	2.993	SPB
V136	4.379	-2.14100	-4.6030	3.734	$\beta$ Cep
V138	4.428	-2.39100	-5.9480	4.272	$\beta$ Cep
V139	4.041	-0.29690	-0.2839	2.006	SPB
V140	4.177	-1.18000	-1.3790	2.444	SPB
V142	4.136	-0.81250	-0.1195	1.941	SPB
V145	4.061	-0.43750	-0.2515	1.993	new
V150	4.090	-0.64840	-1.3020	2.414	SPB
V153	4.301	-1.70300	-2.5100	2.897	SPB
V156	4.246	-1.30500	-2.8010	3.013	SPB
V157	4.087	-0.71880	-0.3117	2.017	SPB

al. (2013) analyzed the population of periodic variable stars in the open cluster NGC 3766. They found a large population of new variable stars between SPB stars and the  $\delta$  Scuti stars, the region where no pulsations were predicted based on the standard stellar models. The periods of these variable stars ranges from 0.1 to 0.7 d, with amplitudes between 1.0 to 4.0 mmag. They found that 20% stars are variable in that region within their detection limit and expected more stars to be variable in this region. The origin of variability of these stars could be pulsation. One of the probable causes of pulsation in these stars could be rapid rotation which alter the internal conditions of a star enough to sustain stellar pulsations. The second cause for the brightness variation in these stars might be the presence of spots on the surface of such rotating stars and that these spots would induce light variations as the star rotates. But hot stars are not expected to be active, and no theory can currently explain how spots could be produced on the surface of such stars. Balona et al. (2011) did not find any star lying between red end of the SPB stars and blue end of  $\delta$  Scuti type stars.

On the basis of distribution of variables in the  $H - R$  diagram (Fig. 10) we classified 3 stars as  $\beta$  Cep, 25 stars as

**Figure 8.** Same as Fig. 6 but for field variable stars. The complete figure is available electronic form only.

SPB and 17 stars as new class. The classification is mentioned in the last column of Table 3. Present sample of MS variable stars consists of 17 stars which lie below the red end of SPB variables. These stars might have similar kind of variability characteristics like the new class of variables detected by Mowlavi et al. (2013) in the case of open cluster NGC 3766. The variables classified on the basis of the  $H - R$  diagram (cf. Fig. 10) are given in the last column of Table 3. The periods of new class variables range from 0.17 to 0.58 d. The amplitude of their brightness variation varies from 0.007 to 0.019 mag. Out of 17 stars four stars numbered V74, V91, V104 and V109 were detected spectroscopically as B-type star by Marco & Negueruela (2002 a, b). The detection of 17 new class variables supports the finding of Mowlavi et al. (2013).

Twenty five MS stars are lying in the instability region of SPB stars. Only 20 stars namely V69, V78, V82, V83, V88, V92, V94, V97, V104, V117, V121, V125, V126, V132, V133, V139, V140, V150, V153 and V156 classified as SPB stars have periods in the range of 0.4 to 0.6 d. The amplitude of these stars varies from 0.006 to 0.021 mag. Their variability characteristics reveal that these could SPB type stars. The periods estimated for the remaining MS variable stars (V112, V128, V135, V142 and V157) distributed in the instability region of SPB stars are less than 0.40 d. Star V133 could be probably classical Be star (Marco & Negueruela 2002b) and it is found to be located where new class of variables has been detected by Mowlavi et al. (2013). This star is located in the centre of the cluster NGC 1893 (see Fig. 1). It has a light-curve similar to the Be type stars. Be stars are known to be fast rotating stars. These stars occupy the same region of B-type stars in the  $H - R$  diagram. Therefore it becomes difficult to separate them from normal B-type stars.

The present variable sample consists of 3 stars which lie in the  $\beta$  Cep region in the  $H - R$  diagram and these could be most probably  $\beta$  Cep type variables. Majewska-



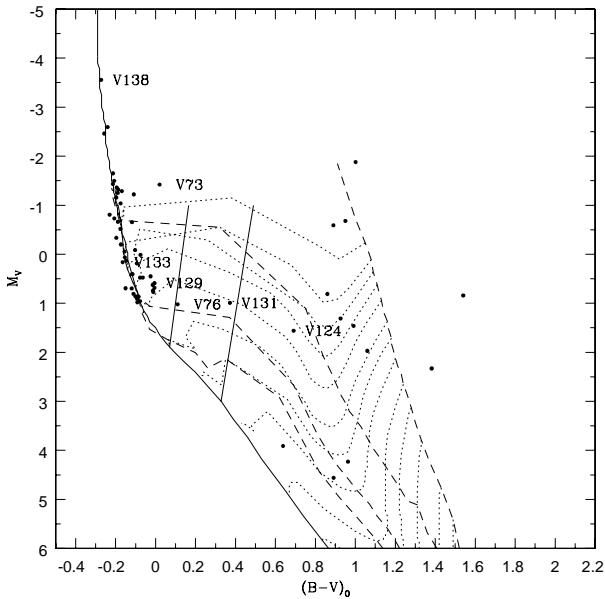


**Figure 9.**  $M_V/(B-V)_0$  colour-magnitude diagram for the MS and PMS stars of the cluster NGC 1893. The ZAMS by Girardi et al. (2002) and PMS isochrones for 0.1, 1, 5, 10 Myrs by Siess et al. (2000) are shown. The dotted curves show PMS evolutionary tracks of stars of different masses. The classical instability strip of Cepheids is taken from the literature (see Zwintz & Weiss 2006). The stars labeled are discussed in section 6.

Świerzbiniowicz et al. (2008) presented photometry of stars in cluster *h* and  $\chi$  Persei (NGC 869 and 884) and found a number of  $\beta$  Cep, B and Be type stars. They found some stars which show multiperiodic pulsations, indicating  $g$  modes or other modes that occur in the presence of fast rotation. The cause of variability in B type stars can be understood in terms of Opacity ( $\kappa$ ) mechanism which is a process that drives pulsations in stars. Opacity mechanism has been discussed by Eddington (1917), Zhevakin (1953), Cox (1958) and is related to the opacity behaviour in ionisation zones. Ionisation regions or layers correspond to a strong increase in opacity which leads the opacity bumps (see Gastine & Dintrans 2008). The radiation coming from the deeper layers gets blocked in the high  $\kappa$  region. The gas heats and the pressure rises below the layer, pushing it outwards. The layer expands, and becomes more transparent to radiation. Radiation flows through, gas cools, and pressure below the layer drops. The layer falls inwards and the cycle repeats. In case of B type stars observations and theory suggest that the opacity of Iron (Fe) atoms is responsible to drive the observed pulsation. In a star Fe bump is an abundance of iron at a depth where the temperature is very high ( $T=2,00,000$  K). The increase in the opacity of Fe is also known as the Z bump. The photometric variability in SPB and  $\beta$  Cep variables is caused by  $\kappa$  mechanism acting in the metal opacity bump (Dziembowski et al. 1993). Dziembowski et al. (1993) predicted the existence of a large region in the MS band at lower luminosities with the help of opacity mechanism, where high order  $g$  modes are unstable with the periods ranging from 0.4 to 3.5 d. They

also proposed that in other B-type stars having same period range opacity mechanism remains the same. Townsend (2005) found that retrograde mixed modes are unstable in mid to late B-type stars, as a results of the same iron-bump opacity mechanism that is usually associated with SPB and  $\beta$  Cep stars. Le Pennec & Turck-Chièze (2014) investigate that Iron group opacities in the envelope of massive stars seems puzzling. The possible causes responsible for periodic brightness variation in case of most of the MS stars detected in the present study could be pulsations, which occur due to either of fast rotation that somehow alters the internal structure of the star or it could be result of iron-bump opacity mechanism. However, more continuous photometry and spectroscopic observations of NGC 1893 are needed to arrive at any conclusion.

Star V138 is the brightest star in our sample. The spectroscopic study by Marco & Negueruela (2002a) assigned this star a spectral type of O7 V(f). Whereas its absolute magnitude  $M_V$  comes out to be -3.57 mag which results effective temperature of this star as  $\log T_{eff}=4.486$  to 4.405 (Schmidt-Kaler 1982). Thus, derived effective temperature suggests that it might be type B0 or B1. The effective temperature of this star using relation between intrinsic  $(B-V)_0$  colour and effective temperature by Torres (2010) comes out to be  $\log T_{eff}=4.428$ . It shows  $\beta$  Cep-like pulsation. MS stars of spectral type O9 to B2 are very interesting targets to study the internal stellar structure by interpreting the observed oscillation characteristics. These are believed to be progenitors of core-collapse supernovae and chemically enrich the Universe (Saesen et al. 2013). A number of O-type  $\beta$  Cep pulsators have also been detected in ground-based observations (e.g. Telting et al. 2006; De Cat et al. 2007; Pigulski & Pojmański 2008). Blomme et al. (2011) pointed out that the behaviour of the early-type O stars (spectral types O4-O8) is considerably different from that of later-type stars. They found that the earliest O stars show red noise, while the later O-types have pulsational frequencies of the  $\beta$  Cep type. The switch-over occurs around spectral type O8. The specific physical cause of this noise in O-type stars is not clear at present. Previous studies found pulsations in late O-type star while in early O-type star brightness variation could be most possibly because of red noise component. Degroote et al. (2010) detected pulsations in HD 46149 (spectral type O8) and showed that the observed frequency range and spacings are compatible with theoretical predictions. HD 46202 (O9 V) shows clear  $\beta$  Cep-like pulsations (Briquet et al. 2011). HD 47129 (O8 III/I + O7.5 V/III) with a series of frequencies might be a pulsator. But this star has presence of a clear red-noise component as well (Mahy et al. 2011). Observations with the MOST satellite of the O9.5 V star  $\zeta$  Oph also show  $\beta$  Cep-type pulsations (Walker et al. 2005). The shape of light curves, amplitude and period suggest that star V138 could be a  $\beta$  Cep type star. In the  $H-R$  diagram it is found to be located near the instability strip of the  $\beta$  Cep variables.

## 6.2 PMS variables

The majority of the PMS variables detected in the present study have masses  $\lesssim 3 M_\odot$  and these variables could be TTSS. The estimated periods of these probable TTSSs are in the range of 0.187 to 0.528 d. The amplitude of the probable

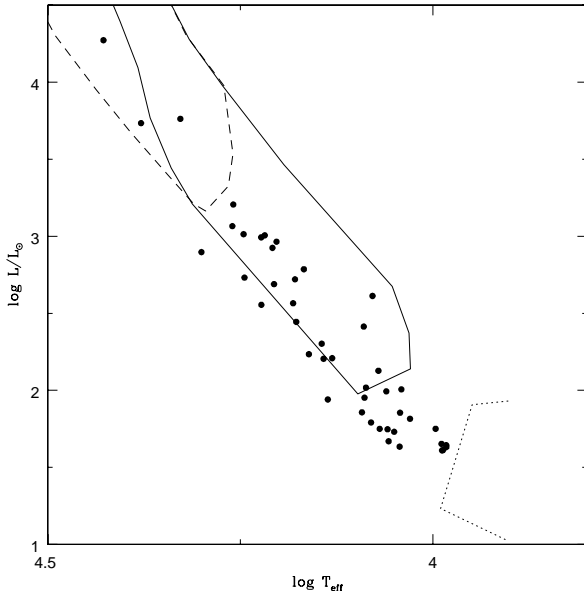


**Figure 10.**  $\log(L/L_{\odot})/\log T_{eff}$  diagram for the cluster NGC 1893. The theoretical SPB instability strip (continuous curve), empirical  $\delta$  Scuti instability strip (dotted curve) and the location of  $\beta$  Cep stars (dashed curve) are taken from the literature (see Balona et al. 2011; references therein).

PMS variable stars ranges from 0.007 and 0.079 mag. The periodic variations in TTs are believed to occur due to the axial rotation of a star with an inhomogeneous surface, having either hot or cool spots (Herbst et al. 1987, 1994). These stars follow the relation of amplitude and mass as mentioned in Lata et al. (2011, 2012).

Stars V129 and V131 were identified as PMS stars by Marco & Negueruela (2002b). Star V129 could be B-type MS star on the basis of its location in  $(J-H)/(H-K)$  TCD. Its variability characteristics also reveal it to be a B-type pulsating star. The location of star V131 in  $(J-H)/(H-K)$  TCD also suggests it to be a PMS star. It could be an Herbig Ae/Be star. Its light curve shows periodic variation of about 0.208 d. Star V73 could also be an Herbig Ae/Be star on the basis of its location in  $(J-H)/(H-K)$  TCD and variability characteristics. The location of star V76 in  $(J-H)/(H-K)$  TCD also suggests that it could also be an Herbig Ae/Be star. In  $M_V/(B-V)_0$  colour magnitude diagram V76 and V131 lie in the classical instability strip of Cepheids. It is believed that the Herbig Ae/Be stars show photometric variability as they move across the instability region in the  $H-R$  diagram on their way to the MS (see Lata et al. 2011 and references therein). Star 124 was selected as the emission-line PMS object because of the presence of emission lines in its spectrum by Marco & Negueruela (2002b). They also find that its spectrum shows weak  $H\alpha$  in emission and its spectral type ranges F9V or G0V. In the  $(J-H)/(H-K)$  TCD it is found to be lying in the ‘F’ region where field stars or Class III sources are found to be located.

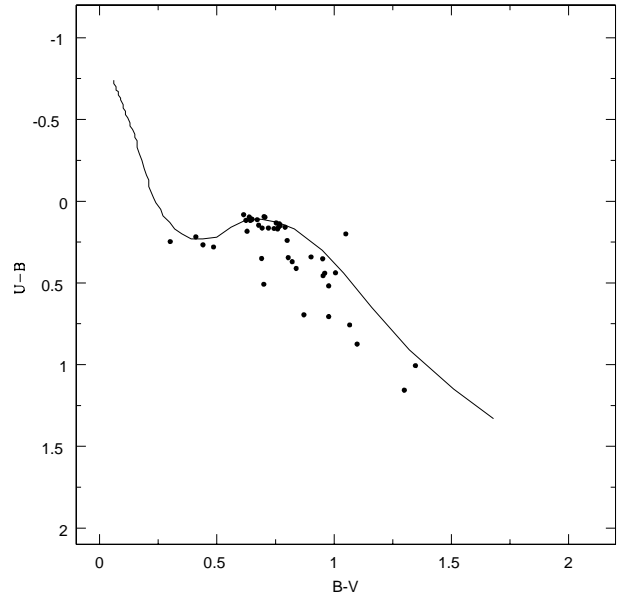


**Figure 11.** The  $(U-B)/(B-V)$  TCD for the field stars. The continuous curve represents ZAMS by Girardi et al. (2002) for the foreground field population having  $E(B-V) = 0.30$  mag.

### 6.3 Field population: variable stars

The present variable sample consists of 43 variable candidates which could be field star population towards the direction of NGC 1893 region. The  $(U-B)/(B-V)$  TCD for the field stars shown in Fig. 11 indicates that these variables are foreground population with  $E(B-V) \sim 0.30$  mag. The variability characteristics of field star population indicates that all of them are short period variables with their amplitude ranging from 0.01 to 0.005 mag. These could be short period variables like  $\delta$  Scuti stars.

## 7 X-RAY LUMINOSITY VS. PERIOD

Most of the MS stars are known to emit X-rays. It is believed that massive and hot stars emit X-rays due to shocks in their winds or collisions between the wind and circumstellar material (see Wright et al. 2011). In late type MS stars the stellar magnetic dynamo is thought to be responsible for the X-rays. A strong correlation between X-ray luminosity and rotation period of the late type MS stars has been found (Walter & Bowyer 1981; Pallavicini et al. 1981; Pizzolato et al. 2003). Though the present MS variable candidates belong to upper region of the MS in the  $H-R$  diagram, we explored the correlation between X-ray luminosity ( $L_X$ ) and period of MS stars (filled circles) and field stars (filled triangles) in Fig. 12. The  $L_X$  values have been taken from the Caramazza et al. (2012). In Fig. 12 we have also plotted the  $L_X$  and rotation period for stars (open circles) taken from Pizzolato et al. (2003). A comparison indicates that present data seem to follow the general trend represented by the Pizzolato et al. (2003), however the  $L_X$  of the present sample is systematically higher as compared to that of Pizzolato et al. (2003).

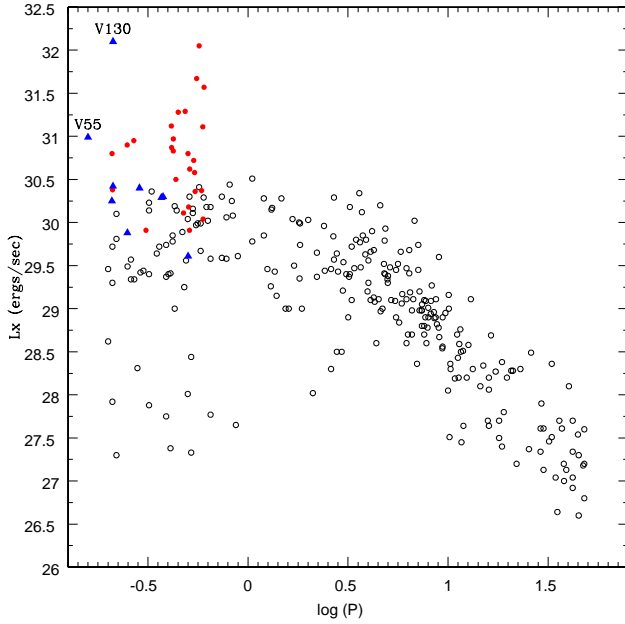


**Figure 12.** X-ray luminosity vs period for variable stars. Filled circles (MS stars), filled triangles (field stars) and open circles represent present sample and that taken from Pizzolato et al. (2003).

sample. It is expected as the star in the present sample has mass  $2.7 \lesssim M/M_{\odot} \lesssim 16.0$  whereas the sample by Pizzolato et al. (2003) has mass in the range of 0.6 to  $1.3 M_{\odot}$ . It is well known that  $L_X$  depends on the stellar mass (see e.g. Pizzolato et al. 2003; Pandey et al. 2014). The X-ray emission of present sample lies in the saturated region, hence it appears to be dependent on the characteristics of the stellar structure (cf. Pizzolato et al. 2003). Fig. 12 also indicates that a few field stars like V130 and V55 have higher  $L_X$ , suggesting that these field stars could be massive ones and these could be most probably B type variables.

## 8 SUMMARY

The paper presents the light curves of 104 variable candidates in the young open cluster NGC 1893. Among 104 variable candidates 45 stars could be MS variables. The periods of MS variables ranges from  $\sim 0.15$  to  $\sim 0.6$  d with brightness variation of  $\lesssim 0.02$  mag. We classified 3 stars as  $\beta$  Cep, 25 stars as SPB stars and 17 stars as new class type stars (cf. Mowlavi et al. 2013) on the basis of their location in the  $H - R$  diagram. We have also found 16 stars as variables which could be of PMS nature. Additionally, there are 43 stars which might belong to the field star population. The correlation between X-ray luminosity ( $L_X$ ) and period of MS stars follows the general trend as given by Pizzolato et al. (2003).

## 9 ACKNOWLEDGMENT

We are thankful to the anonymous referee for useful comments which have improved the contents and presentation of the paper.

## REFERENCES

- [ Balona L. A., Dziembowski W. A., Pamyatnykh A., 1997, MNRAS, 289, 25
- [ Balona L. A., Pigulski A., Cat P. De, Handler G., Gutiérrez-Soto J., Engelbrecht C. A., Frescura F., Briquet M., et al, 2011, MNRAS, 413, 2403
- [ Bessell M. S., Brett J. M., 1988, PASP, 100, 1134
- [ Blomme R., Mahy L., Catala C., Cuypers J., Gosset E., Godart M., Montalbán J., Ventura P., Rauw G., Morel T., 2011, A&A, 533, 4
- [ Briquet M., De Cat P., Aerts C., Scuflaire R., 2001, A&A, 380, 177
- [ Briquet M.; Aerts C., Baglin A., Nieva M. F., Degroote, P., et, 2011, A&A, 527, 112.
- [ Caramazza M., Micela G., Prisinzano L., Sciortino S., Damiani F., Favata F., Stauffer J. R., Vallenari A., Wolk S. J., 2012, A&A, 539, 74
- [ Cutri R. M., Skrutskie M. F., van Dyk S., Beichman C. A., Carpenter J. M., Chester T., Cambresy L., Evans T., Fowler J., Gizis J., et al., 2003, 2MASS All Sky Catalog of point sources.
- [ Cohen J. G., Persson S. E., Elias J. H., Frogel J. A., 1981, ApJ, 249, 481
- [ Cox J. P. 1958, ApJ, 127, 194
- [ De Cat P., Briquet M., Aerts C., Goossens K., Saesen S., Cuypers J., Yakut K., Scuflaire R., Dupret M. -A., Uytterhoeven K., et al. 2007, A&A, 463, 243
- [ Degroote P., Briquet M., Auvergne M., Simón-Díaz S., Aerts C., Noels A., Rainer M., Hareter M., Poretti E., Mahy L., et al. 2010, A&A, 519, A38
- [ Diago P. D., Gutiérrez-Soto J., Fabregat J., Martayan C., Suso J., 2008, arXiv0810.0166D.
- [ Dziembowski W. A., Moskalik P., Pamyatnykh A. A., 1993, MNRAS, 265, 588
- [ Dziembowski W. A., Pamiatnykh A. A., 1993, MNRAS, 262, 204
- [ Eddington A. S., 1917, The Observatory, 40, 290
- [ Gautschi A., & Saio H., 1993, MNRAS, 262, 213
- [ Gastine T., & Dintrans B., 2008, A&A, 484, 29
- [ Girardi L., Bertelli G., Bressan A., Chiosi C., Groenewegen M. A. T., Marigo P., Salasnich B., & Weiss A., 2002, A&A, 391, 195
- [ Gruber D., Saio H., Kuschnig R., Fossati L., Handler G., Zwintz K., Weiss W. W., Matthews J. M., et al, 2012, MNRAS, 420, 291
- [ Gutierrez-Moreno A., 1975, PASP, 87, 805
- [ Handler G., Tuvikene T., Lorenz D., Shobbrook R. R., Saesen S., Provencal J. L., Pagani M., Quint B., Desmet M., Sterken C., Kanaan A., Aerts C., 2008, CoAst, 157, 315
- [ Handler G., Meingast S., 2011, A&A, 533, 70
- [ Herbst W., Booth J. F., Koret D. L., Zajtseva G. V., Shakhovskaya H. I., Vrba F. J., Covino E., Terranegra L., Vittone A., Hoff D., et al., 1987, AJ, 94, 137

- [ ] Herbst W., Herbst D. K., Grossman E. J., Weinstein D., 1994, *AJ*, 108, 1906
- [ ] Jerzykiewicz M., Kopacki G., Pigulski A., Koaczkowski Z., Kim S. -L., 2011, *AcA*, 61, 247
- [ ] Jerzykiewicz M., Kopacki G., Molenda-Zakowicz J., Kolaczowski Z., 2003, *AcA*, 53, 151
- [ ] Kiriakidis M., El Eid M. F., Glatzel W., 1992, *MNRAS*, 255, 1
- [ ] Luo Y. P., Zhang X. B., Deng L. C., Han Z. W., 2012, *ApJ*, 746, 7
- [ ] Lata S., Pandey A. K., Chen W. P., Maheswar G., Chauhan N., 2012, *MNRAS*, 427, 1449
- [ ] Lata S., Pandey A. K., Maheswar G., Mondal S., Kumar B., 2011, *MNRAS*, 418, 1346
- [ ] Le Pennec M.; Turck-Chièze S., 2014, *IAUS*, 301, 229
- [ ] Lenz P., Breger, M., 2005, *Comm. Asteroseismol.*, 146, 53
- [ ] Lomb N.R., 1976, *ApSS*, 39, 447
- [ ] Landolt A. U., 1992, *AJ*, 104, 340
- [ ] Majewska-Świerzbiniowicz A., Pigulski A., Szabó R., Csabry Z., 2008, *JPhcs*, Vol 118, Issue 1, id. 012068
- [ ] Mahy L., Gosset E., Baudin F., Rauw G.; Godart M., Morel T., Degroote P., Aerts C., Blomme R., Cuypers J., et al. 2011, *A&A*, 525, A101
- [ ] Marco A., Negueruela I., 2002a, *ASPC*, 267, 289
- [ ] Marco A., Negueruela I., 2002b, *A&A*, 393, 195
- [ ] Michalska G., Pigulski A., Stelicki M., Narwid A., 2009, *AcA*, 59, 349
- [ ] Majewska A., Pigulski A., Rucinski S. M., 2008, *CoAst*, 157, 338
- [ ] Mowlavi N., Barblan F., Saesen S., Eyer L., 2013, *A&A*, 554, 108
- [ ] Moskalik P., Dziembowski W. A., 1992, *A&A*, 256, 5
- [ ] McNamara B. J., Jackiewicz J., McKeever J., 2012, *AJ*, 143, 101
- [ ] Massey P., Johnson K. E., Degioia-Eastwood K., 1995, *APJ*, 454, 151
- [ ] Meyer M. R., Calvet N., Hillenbrand L. A., 1997, *AJ*, 114, 288
- [ ] Pandey A. K., Samal M. R., Yadav R. K., Richichi A., Lata Sneh, Pandey J. C., Ojha D. K., Chen W. P., 2014, *NewA*, 29, 18
- [ ] Pigulski A. & Pojmański G. 2008, *A&A*, 477, 917
- [ ] Prisinzano L., Sanz-Forcada J., Micela G., Caramazza M., Guarcello M. G., Sciortino S., Testi L., 2011, *A&A*, 527, 77
- [ ] Pallavicini R., Golub L., & Rosner R., Vaiana G. S., Ayres T., Linsky J. L., 1981, *ApJ*, 248, 279
- [ ] Pizzolato N., A. Maggio A., Micela G., Sciortino S., Ventura P., 2003, *A&A*, 397, 147
- [ ] Sariya D. P., Lata S., Yadav R. K. S., 2014, *NewA*, 27, 56
- [ ] Scargle J.D., 1982, *ApJ*, 263, 835
- [ ] Schmidt-Kaler Th., 1982, *Landolt-Bornstein, Numerical data and Funct. Relationship in Science and Technology*, New Series, Group 6, Vol. 2b, p. 453
- [ ] Saesen S., Carrier F., Pigulski A., Handler G., Narwid A., Fu J. N., Zhang C., Jiang X. J., Vanautgaerden J., et al. 2010, *A&A*, 515, 16
- [ ] Saesen S., Briquet M., Aerts C., Miglio A., Carrier F., 2013, *AJ*, 146, 102
- [ ] Stankov A. & Handler G. 2005, *ApJS*, 158, 193
- [ ] Stetson P. B., 1987, *PASP*, 99, 191
- [ ] Sharma S., Pandey A. K., Ojha D. K., Chen W. P., Ghosh S. K., Bhatt B. C., Maheswar G., Sagar R., 2007, *MNRAS*, 380, 1141
- [ ] Saio H., Kuschnig R., Gautschi A., Cameron C., Walker G. A. H., Matthews J. M., Guenther D. B., et al., 2006, *ApJ*, 650, 1111
- [ ] Siess L., Dufour E., Forestini M., 2000, *A&A*, 358, 593
- [ ] Telting J. H., Schrijvers C., Ilyin I. V., Uytterhoeven K., De Ridder J., Aerts C., Henrichs H. F., 2006, *A&A*, 452, 945
- [ ] Townsend R. H. D., 2005, *MNRAS*, 364, 573
- [ ] Torres G., 2010, *AJ*, 140, 1158
- [ ] Waelkens C., 1991, *A&A*, 246, 453
- [ ] Waelkens C., Aerts C., Kestens E., Grenon M., Eyer L., 1998, *A&A*, 330, 215
- [ ] Walker G. A. H., Kuschnig R., Matthews J. M., Reegen, P.; Kallinger, T.; Kambe, E.; Saio, H.; Harmanec, P.; Guenther, D. B.; Moffat, A. F. J.; et al. 2005, *ApJ*, 623, 145
- [ ] Walter F. M., & Bowyer S. 1981, *ApJ*, 245, 671
- [ ] Wright N. J., Drake J. J., Mamajek E. E., Henry G. W., 2011, *ApJ*, 743, 48
- [ ] Yang Yi, Fu J.-N., Chen X.-D., Yu M., Zhang Y.-P., 2013, *NewA*, 23, 67
- [ ] Zhang C., Fu J. N., Jiang X. J., 2008, *JPhCS*, 118, 2078
- [ ] Zhevakin S. A. 1953, *Russ. A. J.*, 30, 161
- [ ] Zwintz K., Weiss W. W., 2006, *A&A*, 457, 237